Tetrahedron 67 (2011) 8073–8078

Contents lists available at SciVerse ScienceDirect

Tetrahedron

journal homepage: www.elsevier.com/locate/tet

Zinc selective chemosensor based on pyridyl-amide fluorescence

Hong Gyu Lee [a], Ju Hoon Lee [a], Seung Pyo Jang [a,b], Hyun Min Park [a], Sung-Jin Kim [c], Youngmee Kim [c], Cheal Kim [a,*], Roger G. Harrison [b,*]

[a] Department of Fine Chemistry, Seoul National University of Science and Technology, Seoul 139-743, Republic of Korea
[b] Department of Chemistry and Biochemistry, Brigham Young University, Provo, Utah, UT 84602, USA
[c] Department of Chemistry and Nano Science, Ewha Womans University, Seoul 120-750, Republic of Korea

ARTICLE INFO

Article history:
Received 25 June 2011
Received in revised form 17 August 2011
Accepted 18 August 2011
Available online 25 August 2011

ABSTRACT

Chemosensors are developed to image zinc ions. Fluorescence enhancement due to Zn^{2+} binding is an excellent way to detect its presence. A chemosensor for Zn^{2+} based on dipicolylamine (DPA) groups connected by a pyridyl amide backbone has been synthesized. Addition of 2-chloroacetyl chloride to 2,6-diaminopyridine affords 2,6-bis(chloroethylamido)pyridine, which is converted to the sensor **BADPA-P** by 2,2′-dipicolylamine displacement of chlorine. This compound along with two others, the mono-DPA, **ADPA-P** and the benzyl in place of pyridyl, **BADPA-B**, present three potential Zn^{2+} sensors. It was found that **BADPA-P** in the presence of Zn^{2+} shows a large increase in fluorescence, whether in polar organic or aqueous environments. Its fluorescence in the presence of Cd^{2+}, unlike with Zn^{2+}, is not enhanced when excited at longer wavelengths. Proton NMR measurements, indicate two Zn^{2+} ions bind to **BADPA-P**. Also, Zn^{2+} enhances fluorescence even when other metal ions are present.

1. Introduction

After iron, zinc is the most abundant transition metal in living organisms and is used for structure, enzymes, and transcription. The spectroscopic properties of zinc make it difficult to monitor and thus to understand its role in proteins, neurotransmissions, and cell functions. Having a full d-shell of electrons, zinc does not have electron transitions in the visible region of light nor is it paramagnetic. It thus resembles calcium, however, unlike calcium, it binds strongly to nitrogen ligands due to its smaller size, greater effective nuclear charge, and d-orbital overlap. Current research has focused on synthesizing zinc-binding compounds;[1] molecules that when in the presence of zinc show a fluorescence response. Fluorescence changes are often strong and easily detectable.

Several types of molecules have been used as zinc fluorophores. Due to their ease of synthesis and strong zinc binding ability, molecules containing quinoline derivatives have been used.[2] They have shown fluorescence resonance energy transfer (FRET) fluorescence.[3] Other studied molecules include the naphthalenes, which have been attached to Schiff bases,[4] naphthalimides, which have been attached to azamacrocyles,[5] and naphthyridyls, which have been attached to amides.[6] Pyrenes,[7] bipyridines,[8] and imines[9] have also recently been used as fluorophores.

With its two pyridine groups and one amine nitrogen between them, dipicolylamine (DPA) chelates strongly to electropositive Zn^{2+}. The Zn^{2+}—DPA complex is such a good probe that it has been attached to fluorescent molecules and used to image dying cells as well as bacterial infections.[10] Fluorescent sensors for zinc have been formed by using the DPA molecule as the zinc binding domain. For example, a sensor with a DPA group separated from a fluorescent moiety by a methylene group shows fluorescence enhancement in the presence of zinc ions.[11] These molecules have been used to image zinc in living systems. It is proposed that when zinc binds to the lone pair of electrons on the tertiary nitrogen of DPA, it inhibits photoinduced electron transfer (PET). Such an electron transfer would allow a nonradiative decay pathway for the fluorescent moiety and inhibit fluorescence. A variety of properties have been observed when DPA has been attached to quinoline groups. Some of these properties include detection femtomolar zinc,[12] a large Stokes shift,[13] two-photon fluorescence,[14] and ratiometric zinc detection.[15] DPA has also been attached to naphthalimides, which show an internal charge transfer (ICT) mechanism of zinc sensing.[16] Important ratiometric sensors have been synthesized when DPA has been attached to benzoimidazole groups.[17] When an anthracene group is attached to DPA, zinc sensors that fluoresce at biologically relevant pH are realized.[18]

In a few cases, two DPA binding domains are linked together in the same molecule. Some of these molecules have been studied for zinc binding and with phosphate containing moleucles.[19] The zinc binding molecules with two DPA units have shown good fluorescence response to zinc and strong binding.[20]

* Corresponding authors. Tel.: +1 801 422 8096; fax: +1 801 422 0153 (R.G.H.); tel.: +82 2 970 6693; fax: +82 2 973 9149 (C.K.); e-mail addresses: chealkim@seoultech.ac.kr (C. Kim), roger_harrison@byu.edu (R.G. Harrison).

0040-4020/$ – see front matter © 2011 Elsevier Ltd. All rights reserved.
doi:10.1016/j.tet.2011.08.049

In this paper, we give the synthesis and properties of new Zn^{2+} sensors that contain two and one zinc-binding sites (**BADPA-P**, **BADPA-B**, and **ADPA-P**, Scheme 1). DPA moieties are incorporated into the sensors to impose strong zinc binding and promote enhanced fluorescence upon zinc binding. The zinc sensors reported herein are straightforward to synthesize, selective for zinc over other metal ions, including cadmium, and even show fluorescence enhancement in the presence of zinc in aqueous solutions. By studying these three sensors, we have found that two DPA units and a pyridyl ring enhance the fluorescence response due to Zn^{2+}.

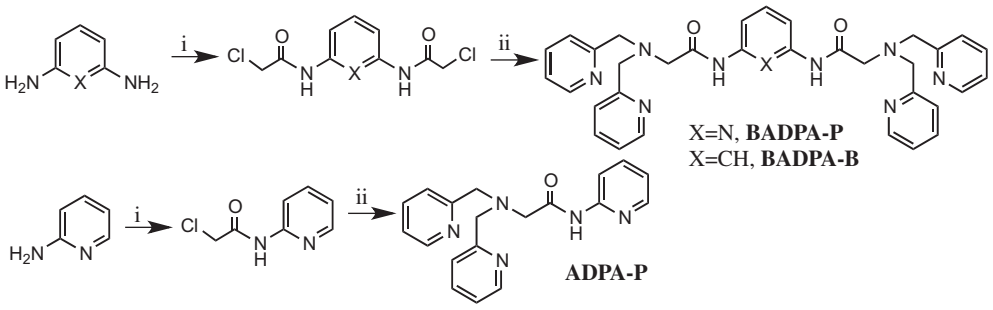

Scheme 1. Synthesis of **BADPA-P**, **BADPA-B**, and **ADPA-P**. (i) $ClCOCH_2Cl$, pyridine, 0 °C, 1 h. (ii) KI, DIPEA, DPA, reflux, 1 day.

2. Results and discussion

2.1. Synthesis

The sensor synthesis begins by forming the pyridine diamide compound by the addition of 2 equiv of 2-chloroacetyl chloride to pyridine-2,6-diamine in the presence of base (Scheme 1). To this compound is added dipicolylamine (DPA) and base to form the **BADPA-P** sensor. The NMR spectrum of the sensor shows all of the expected aromatic, methylene, and amide protons. Replacing pyridine diamine with 1,3-phenylene diamine and adding the same reagents affords the **BADPA-B** sensor (Scheme 1). Its structure is identical to **BADPA-B**, except it lacks nitrogen in the central benzene ring. To investigate the need for two DPA groups, the mono-DPA compound (**ADPA-P**) was synthesized. To form this compound, aminopyridine was added to 2-chloroacetyl chloride in the presence of base, which was further reacted with DPA. These compounds, **BADPA-P**, **BADPA-B**, and **ADPA-P** give a set of molecules that will help us understand the effect of pyridine and two DPA units on the fluorescence enhancement induced by Zn^{2+} binding.

Single crystals of **BADPA-P** were grown and its crystal structure analyzed.[21] The planar amide–pyridine–amide backbone is revealed, with amide carbonyls pointing in the same direction as the pyridine ring (Fig. 1). The pyridines and nitrogens from the DPA form a pocket positioned around the pyridine nitrogen of the backbone. The DPAs are uniquely positioned so as when they bind zinc, the zincs will also be in proximity of the amide oxygens or nitrogens. The crystal structure gives a static picture of the compound and it needs to be noted that the DPA groups could swing around and if so, allow the carbonyl oxygens to bind to zinc as has been shown by similar compounds.[11] The structure of **BADPA-P** gives good reason to predict that zinc binding to the DPA groups should enhance fluorescence due to electron density removal from the amide groups, thus not allowing PET and a nonradiative decay pathway.

2.2. Fluorescence enhancement

The addition of Zn^{2+} to **BADPA-P** causes a large fluorescence enhancement (Fig. 2). As Zn^{2+} is titrated into a solution of **BADPA-P**, the natural fluorescence of **BADPA-P** at 360 nm (Φ=<0.005) due to the pyridyl-amide groups is dwarfed by the new fluorescence at 410 nm (Φ=0.041, excitation at 326 nm). The intensity of the fluorescence grows slowly until 1 equiv of Zn^{2+} is added, at which point its intensity sharply increases until around 2 equiv of Zn^{2+} ions have been added. Since **BADPA-P** has two DPA groups, a first equivalent of Zn^{2+} will bind one DPA, after which the second equivalent of Zn^{2+} will bind the second DPA group. Both DPA groups need to be bound by Zn^{2+} to create the greatest fluorescence enhancement.

When **BADPA-P** is excited at shorter wavelengths (284 and 295 nm) again a new fluorescence peak is observed, but this time it is at lower wavelength, 390 nm, and its intensity is not as great (Fig. S1, Supplementary data). The growth of this peak is preceded by the reduction of the fluorescence of **BADPA-P** at 330 nm, which after one and a half equivalents of Zn^{2+} is completely reduced. Thus, Zn^{2+} binding can be monitored by fluorescence reduction or enhancement. There is an isosbestic point from zero to 1 equiv of Zn^{2+}, which is disrupted upon the addition of more equivalents of Zn^{2+}. This implies direct conversion of **BADPA-P** to a **BADPA-P**–Zn complex, which in turn forms another complex as more Zn^{2+} is added.

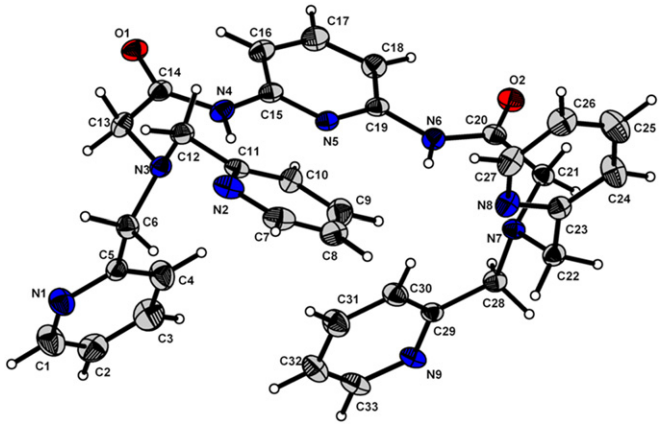

Fig. 1. Crystal structure of **BADPA-P**. Displacement ellipsoids are shown at the 30% probability level.

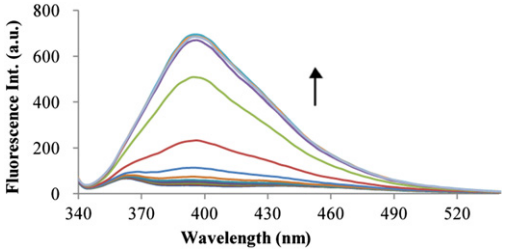

Fig. 2. Fluorescence spectra of **BADPA-P** (10 μM, MeOH) with increasing amounts of Zn^{2+}(0–3 equiv) excited at 326 nm.

The addition of up to 2 equiv of Zn^{2+} results in incremental changes in fluorescence, whether reduction of fluorescence at 330 nm or enhancement at 390 nm. Job plots using fluorescence reveals 2:1 binding of Zn^{2+} to **BADPA-P** (Fig. 3). This change in fluorescence with increasing concentration of zinc, means **BADPA-P** is a potential ratiometric sensor. Since it strongly binds Zn^{2+}, with a predicted K_d close in magnitude to a similar DPA–amide compound, which has a $K_d=10^9$,[11] the fluorescence enhancement caused by Zn^{2+} can be detected at low concentrations. An increase in fluorescence is even detected at micromolar concentrations of Zn^{2+}. Another favorable property of the fluorescence of **BADPA-P** due to Zn^{2+}, is that the fluorescence maximum is at 410 nm and tails off into the visible, thus, visible wavelengths of light can be used to detect zinc ions.

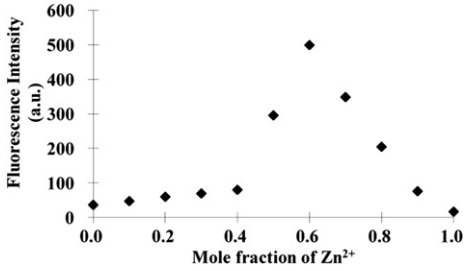

Fig. 3. Job plot using fluorescence of **BADBP-P**. The ratio of fluorescence intensity to fluorescence maximum continues to increase to after 0.6 mole fraction, indicating a 2:1 Zn^{2+} to **BADBP-P** ratio.

The fluorescence of **ADPA-P**in the presence of Zn^{2+} is also increased, however not nearly as great as **BADPA-P** (Fig. 4, Fig. S2, Supplementary data). When excited at 284 and 295 nm its fluorescence nearly doubles after 1 equiv of Zn^{2+} has been added. More equivalents of Zn^{2+} are required to gain the same response when **ADPA-P** is excited at 313 nm. Fluorescence enhancement is also observed when Zn^{2+} is added to **BADPA-B**, but as with **ADPA-P**, the increase is not as pronounced as it is with **BADPA-P** (Fig. S3, Supplementary data). Although the most dramatic increase in fluorescence is observed upon adding up to 2 equiv of Zn^{2+}, more equivalents of Zn^{2+} continue to cause a fluorescence increase.

Noting the fluorescence enhancement due to Zn^{2+} in methanol solutions, a more aqueous environment was attempted, one potentially more biologically relevant. Adding Zn^{2+} to a buffered solution of **BADPA-P** in methanol/water or water, causes fluorescence enhanced (Fig. 5). However, when Zn^{2+} is added to **ADPA-P** and **BADPA-B**, fluorescence enhancement in aqueous environments is not observed (Fig. S4, Supplementary data). This is most likely due to **BADPA-P**–Zn absorbing longer, 326 nm wavelength light, while **ADPA-P**–Zn and **BADPA-B**–Zn complexes do not absorb at this wavelength. The pH of the **BADPA-P** solution affects its fluorescence (Fig. 6). The maximum fluorescence is observed from pH 6 to 7, which is in the biological pH range.

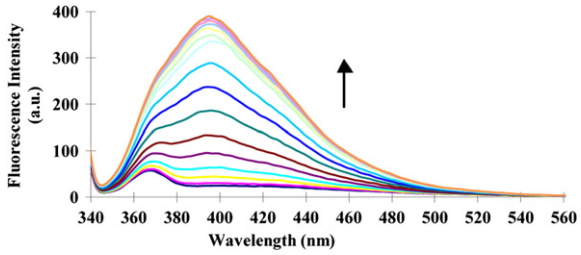

Fig. 5. Fluorescence spectra of **BADPA-P** (20 μM H_2O solution) with increasing amounts of Zn^{2+}(0–60 μM) excited at 326 nm.

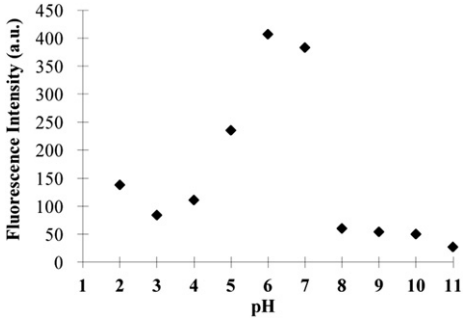

Fig. 6. pH effect on fluorescence of **BADPA-P**. The fluorescence of **BADPA-P** (20 μM in buffered water) in the presence of Zn^{2+} (40 μM) reaches a maximum from pH 6 to 7.

2.3. Absorbance change

The UV–vis absorption changes of **BADPA-P** with Zn^{2+} are minor, but significant (Fig. 7). There is a slight increase in the band at 260 nm, a decrease in the band at 292 nm, and a new band that grows in at 312 nm. The increase of the band at 312 nm means that in the presence of Zn^{2+}, **BADPA-P** becomes fluorescent when excited at 326 nm, even though it normally would not be. Indeed,

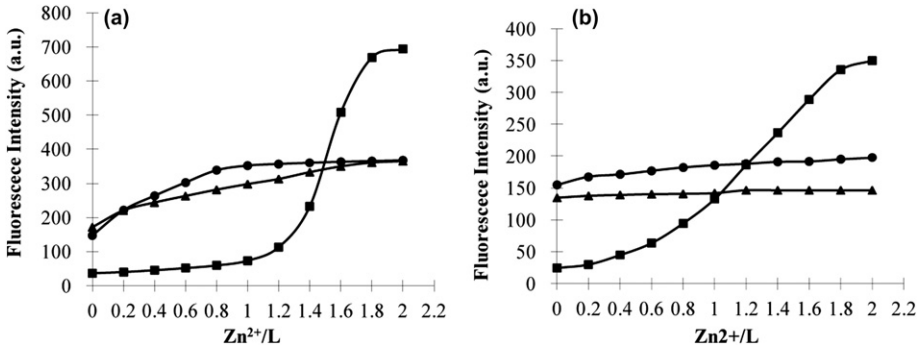

Fig. 4. Comparison of fluorescence enhancement of **BADPA-P** (■), **BADPA-B** (▲), and **ADPA-P** (●) in the presence of Zn^{2+} excited at 326 nm. (a) Sensors are 10 μM methanol solutions with up to 2 equiv of added Zn^{2+}. (b) Sensors are 20 μM **BADPA-P**, 15 μM **BADPA-B**, and 10 μM **ADPA-P** buffered water solutions with up to 2 equiv of added Zn^{2+}.

with the occurrence of this band, the excitation of **BADPA-P** can be done with lower energy light.

The UV–vis absorption spectra for **ADPA-P** are similar to **BADPA-P**, except its two major absorption bands are blue shifted (Fig. S5, Supplementary data). **ADPA-P** only has one amide arm and does not have the length of conjugation of **BADPA-P** and thus has absorbance bands of greater energy. When Zn^{2+} is added to **ADPA-P**, its absorbance at 240 nm is decreased, its absorbance at 260 nm is increased, and it has a new band grow in at 295 nm. This new band is reminiscent of **BADPA-P**, which had a band grow in at 312 nm.

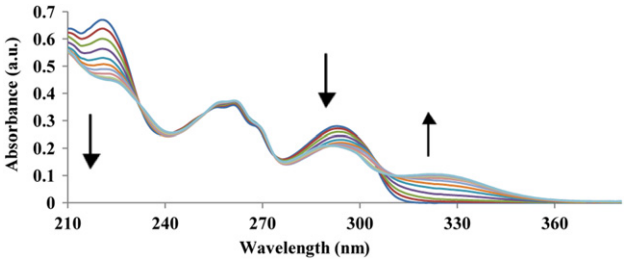

Fig. 7. UV–vis of **BADPA-P** (20 μM, MeOH) with added Zn^{2+}(0–28 μM).

BADPA-B, even though having two amid arms like **BADPA-P**, has only one main absorption band at 240 nm and a shoulder at 260 nm (Fig. S6, Supplementary data). Upon Zn^{2+} addition, its band at 240 nm decreases and its band at 260 nm increases slightly. These bands being at higher energy than those seen in **BADPA-P**, result in lower Zn^{2+} induced fluorescence enhancement when **BADPA-B** is excited at longer wavelengths (326 nm).

2.4. Zn^{2+} binding mode

Monitoring the **BADPA-P**–Zn complexes by NMR shows a stable complex is formed after 2 equiv of Zn^{2+} have been added to **BADPA-P**. As Fig. 8 shows, the well resolved proton NMR peaks of **BADPA-P** broaden and shift upon addition of Zn^{2+} until 2 equiv of Zn^{2+} have been added. For example, the methylene protons of **BADPA-P** are a singlet at 4.0 ppm when Zn^{2+} is not present, but as Zn^{2+} is added they broaden, get lost in the baseline, move to 4.5 ppm and resolve into two doublets. The other **BADPA-P** proton resonances perform similar movements, however the N–H proton resonance moves downfield and splits into a couple of peaks before becoming on singlet. This proton must be in several environments before the final product. This indicates dynamic **BADPA-P**–Zn complexes are present until 2 equiv of Zn^{2+} are present. The proton peaks of **ADPA-P** and **BADPA-B** act in a similar to those of **BADPA-P**, except **ADPA-P** only requires 1 equiv of Zn^{2+} to result in the peaks becoming resolved (Fig. S7, Supplementary data).

The degree of movement of the N–H peak indicates whether zinc ions coordinate to the amide nitrogen or oxygen.[11,22] The N–H resonance of **BADPA-P** in DMSO moves slightly upfield (10.9–10.88 ppm). The N–H peak of **BADPA-B** moves slightly upfield also (10.8–10.7 ppm), while **ADPA-P** moves downfield from 10.8 to 11.3 ppm. As has been observed in other DPA–amide compounds, large chemical shift changes (1 ppm) are indicative of Zn^{2+} binding to amide oxygen, while small changes in the chemical shift of the N–H peak are indicative of Zn^{2+} binding to the amide nitrogens.[11,22] Due to the observed small changes, we conclude that for **BADPA-P**, **BADPA-B**, and **ADPA-P**, Zn^{2+} binds to the nitrogens (Scheme 2).

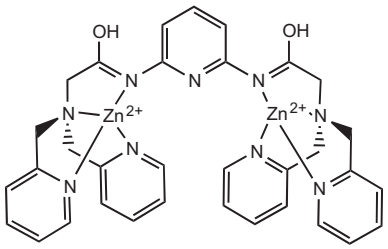

Scheme 2. Proposed Zn^{2+} binding to **BADPA-P** from ^1H NMR chemical shift changes.

2.5. Zn^{2+} selectivity over other metals

Another important aspect of a zinc sensor is its selectivity for Zn^{2+}. When other metal ions are added to **BADPA-P**, such as Na^+, K^+, Ca^{2+}, and Mg^{2+}, they do not affect the fluorescence, while others, such as Fe^{2+}, Mn^{2+}, Cr^{2+}, Co^{2+}, and Ni^{2+} quench the fluorescence. The fluorescence enhancement of **BADPA-P** by Zn^{2+} is 5 times greater than the enhancement by other metal ions when excited at 326 nm (Fig. 9). This remarkable selectivity for Zn^{2+} is

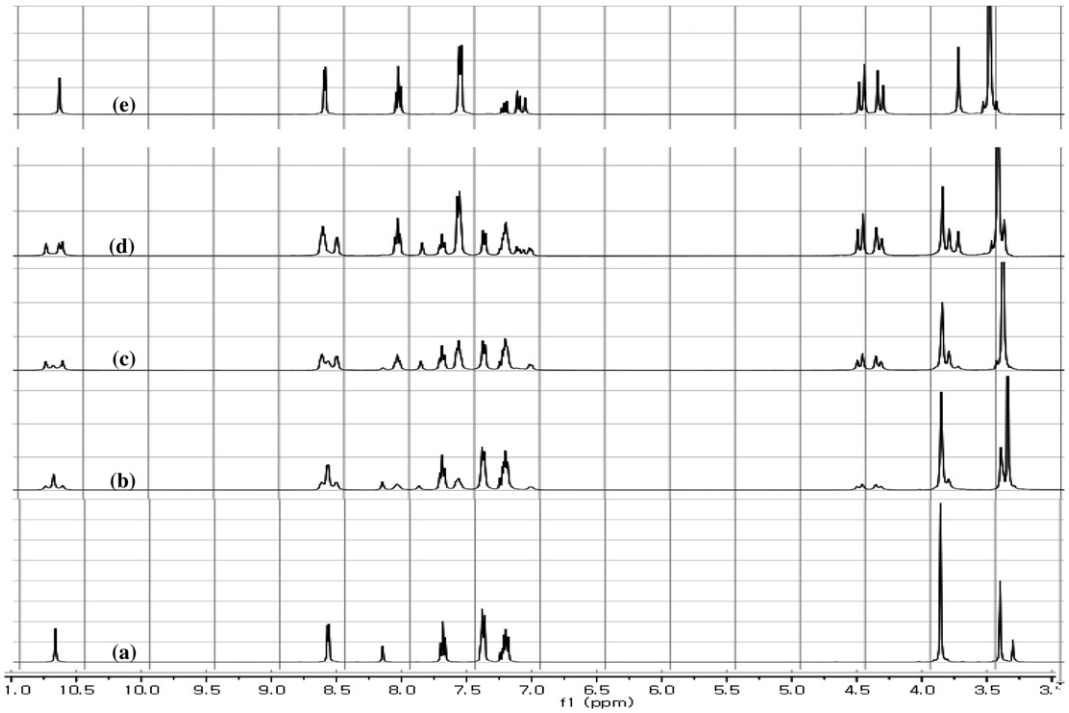

Fig. 8. ^1H NMR changes of **BADPA-P** with added Zn^{2+} in deuterated acetonitrile. Each spectrum is of a sample of **BADPA-P** and (a) 0 (b) 0.5 (c) 1.0 (d) 1.5, and (e) 2.0 equiv of Zn^{2+}. The N–H resonance at 10.7 ppm moves only slightly. The methylene resonances of DPA start at 3.8 ppm, shift downfield and split into doublets, indicating Zn^{2+} binding to DPA.

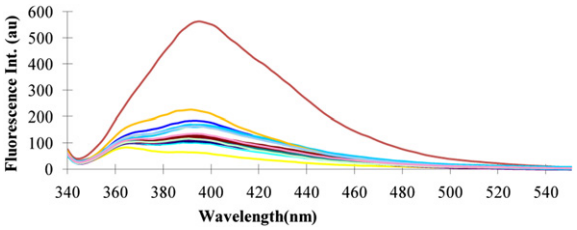

Fig. 9. Fluorescence of **BADPA-P** (10 μM) with Zn^{2+}(20 μM) (top), Cr^{2+} (second), Fe^{2+} (third), Cu^{2+} (lowest) and other metal ions (20 μM) in methanol solution.

explained by Zn^{2+} binding strongly to the DPA groups and stopping the nonradiative decay pathway. Compared to other Zn^{2+} sensors,[11,14,15] **BADPS-P** shows good sensitivity for Zn^{2+} and does not show fluorescence enhancement, even in the presence of Cd^{2+}.

The fluorescence of a sensor, that is, enhanced by Zn^{2+} is often also enhanced by Cd^{2+}. When Cd^{2+} is added to **BADPA-P** and excited at 326 nm, fluorescent enhancement is not observed. However, fluorescent enhancement is induced by Cd^{2+} when **BADPA-P** is excited at shorted wavelengths of light (Fig. S8, Supplementary data). This Zn^{2+} selectivity is most likely due to the **BADPA-P**–Zn complex having a lower energy absorption than the **BADPA-P**–Cd complex. Thus, exciting at lower energy is sufficient to observe fluorescence by Zn^{2+} but does not show fluorescence by Cd^{2+}. Also, the fluorescence of **BADPA-P** in the presence of Zn^{2+} is red shifted from where it is when Cd^{2+} is present (284 nm excitation, Fig. S8, Supplementary data). Thus if an excitation wavelength of higher energy is used, Zn^{2+} and Cd^{2+} could possibly be distinguished by the wavelength of the fluorescence.

Along with showing a greater fluorescent response in the presence of Zn^{2+}, **BADPA-P** also shows selectivity for Zn^{2+} over other metal ions. When metal ions are added to a solution of **BADPA-P** and Zn^{2+}, the fluorescence enhancement caused by Zn^{2+} is retained with K^+, Na^+, Ca^{2+}, Mg^{2+}, Mn^{2+}, Fe^{2+}, Ni^{2+}, Co^{2+}, and Ag^+(Fig. 10). Some metal ions, such as Cd^{2+}, Cu^{2+}, Cr^{2+}, and Hg^{2+}, do compete with Zn^{2+} in binding **BADPA-P**. If these metal ions are present, they might interfere with the detection of zinc. However, they would not give a false positive because they do not enhance the fluorescence of **BADPA-P**. In biological systems, where Zn^{2+} is prevalent, Cd^{2+}, Cr^{2+}, and Hg^{2+} are not present or are in very trace amounts, and thus would not affect the analysis of Zn^{2+}. Mg^{2+} is present in biological environments in much greater concentrations than Zn^{2+}. Under our conditions it does not affect the fluorescence of the **BADPA-P**–Zn^{2+} complex, but further testing needs to be done to check its affect under higher concentrations. Cu^{2+} is biologically relevant, but is approximately one hundred times less concentrated than Zn^{2+} and is bound up in the cell. If released, it would quench the fluorescence of **BADPA-P** and not enhance it.

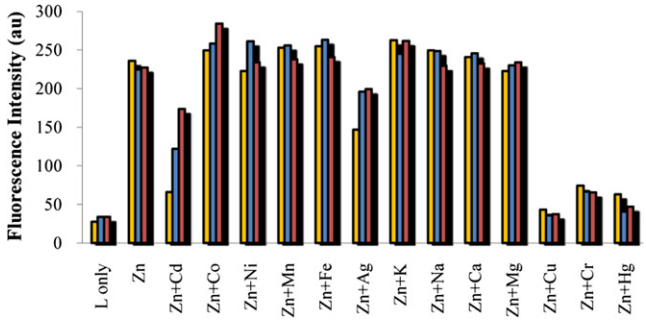

Fig. 10. Fluorescence of **BADPA-P**(5 μM) with two (yellow), 10 (gray), and 20 (red) equivalents of Zn^{2+} and 2 equiv of another metal ion in methanol solution.

3. Conclusion

A new easily synthesized Zn^{2+} sensor (**BADPA-P**) is reported that has DPA groups connected by pyridyl amides. A strong fluorescence enhancement is observed when Zn^{2+} binds **BADPA-P**. NMR data show that two Zn^{2+} ions bind to the sensor. The sensor is selective for Zn^{2+} over Cd^{2+} and other metal ions when excited at 326 nm. Zn^{2+} also competes favorably for **BADPA-P** when in the presence of other metal ions.

4. Experimental

4.1. General methods

Reagents and solvents were purchased from commercial suppliers and used as received. Absorption spectra were recorded at 25 °C using a Perkin–Elmer model Lambda 2S UV–vis spectrometer. ^{1}H NMR measurements were performed on a Varian 400 MHz spectrometer. Fluorescence measurements were performed on a Perkin–Elmer model LS45 Fluorescence spectrometer. X-ray diffraction data were collected on a Bruker SMART AXS diffractometer. Elemental analysis for carbon, nitrogen, and hydrogen was carried out by using a vario MACRO (Elemental Analysensysteme, Germany) in the Laboratory Center of Seoul National University of Science and Technology, Korea.

4.2. Synthesis

4.2.1. 2,6-Bis(chloroethylamido)pyridine. 2-Chloroacetyl chloride (1.25 mL, 16.0 mmol) was dissolved in chloroform (20 mL), then added dropwise to a cooled, stirred solution of pyridine-2,6-diamine (445.4 mg, 4.0 mmol) and pyridine (0.82 mL, 10.0 mmol) in chloroform (20 mL) within 15 min. After stirred for 4 h at room temperature, the liquid was removed under reduced pressure to obtain a pale brown solid. The solid was purified by silica gel column chromatography using DCM/methanol (20:1, v/v) as eluent to afford 524 mg of product (50% yield). IR (KBr): 3385 (N–H), 3362 (N–H), 1689 (C=O), 1591, 1525, 1460, 1398, 1315, 1244, 1155, 807, 780 cm^{-1}. ^{1}H NMR (DMSO-d_6, 300 MHz) δ 10.48 (s, 2H), 7.8–7.75 (m, 3H), 4.35 (s, 4H). ^{13}C NMR (DMSO-d_6, 300 MHz): δ 168.2, 150.5, 141.3, 110.2, 44.2. Anal. Calcd for $C_9H_9Cl_2N_3O_2$ (262.09): C, 41.24; H, 3.46; N, 16.03%. Found: C, 41.58; H, 3.66; N, 16.03%.

*4.2.2. 2,6-Bis(amidomethyl-2,2′-dipicolylamine)pyridine (**BADPA-P**).* 2,6-Bis(chloroethylamido)pyridine (524 mg, 2.0 mmol), 2,2′-dipicolylamine (0.95 mL, 5.0 mmol), *N*,*N*-diisopropylethylamine (0.89 mL, 5.0 mmol), and potassium iodide (50 mg) were added to acetonitrile (30 mL). The solution was refluxed for 12 h under nitrogen atmosphere, cooled to room temperature and placed under reduced pressure to obtain a red-brown oil. The oil was purified by silica gel column chromatography using DCM/methanol (10:1, v/v) as eluent to afford 705 mg of solid product (60% yield). ^{1}H NMR (DMSO-d_6, 300 MHz) δ 10.94 (s, 2H), 8.59 (d, 4H), 7.76–7.67 (m, 7H), 7.47 (d, 4H), 7.20 (t, 4H), 3.99 (s, 8H), 3.51 (s, 4H). ^{13}C NMR (DMSO-d_6, 300 MHz): δ 1701.0, 159.0, 150.7, 149.8, 140.8, 137.3, 123.6, 123.0, 109.9, 60.5, 58.8. FABMS m/z (M^+): calcd 587.67, found, 587.67. Anal. Calcd for $C_{33}H_{33}N_9O_2$ (587.67): C, 67.44; H, 5.66; N, 21.45; O, 5.44%. Found: C, 67.75; H, 5.34; N, 21.62%.

4.2.3. 2,6-Bis(chloroethylamido)benzene. 2-Chloroacetyl chloride (0.784 mL, 10.0 mmol) was dissolved in chloroform (15 mL), then added dropwise to a cooled, stirred solution of 1,3-phenylene diamine (441 mg, 4.0 mmol) and pyridine (0.82 mL, 10.0 mmol) in chloroform (20 mL). The white solid that immediately precipitated was filtered, dried and yielded 896.7 mg (85.8% yield) of product. IR (KBr): 3270 (N–H), 3222, 3095, 1672 (C=O), 1613, 1553, 1485, 1436,

1295, 1235, 961, 880, 789 cm^{-1}. ^1H NMR (DMSO-d_6, 300 MHz) δ 10.35 (s, 2H), 7.95 (s, 1H), 7.34–7.25 (m, 3H), 4.25 (s, 4H). ^{13}C NMR (DMSO-d_6, 300 MHz): δ 165.4, 139.6, 129.87, 115.5, 111.1, 44.3. Anal. Calcd for $C_{10}H_{10}Cl_2N_2O_2$ (261.10): C, 46.00; N, 10.73; H 3.86%. Found: C, 45.83; N, 10.71; H, 3.86%.

*4.2.4. 2,6-Bis(amidomethyl-2,2′-dipicolylamine)benzene (**BADPA-B**).* 1,3-Bis(chloroethylamido)benzene (522.2 mg, 2.0 mmol), 2,2′-dipicolylamine (0.95 mL, 5.0 mmol), *N*,*N*-diisopropylethylamine (0.89 mL, 5.0 mmol), and potassium iodide (50 mg) were dissolved in acetonitrile/DMF (5:1, v/v, 36 mL). After stirred and refluxed for 12 h under nitrogen atmosphere, the mixture was cooled to room temperature and the solvent was removed under reduced pressure to obtain a brown oil. The oil was purified by silica gel column chromatography using DCM/methanol (5:1, v/v) as eluent to afford 737.6 mg (62.0% yield) of product. ^1H NMR (DMSO-d_6, 300 MHz) δ 10.75 (s, 2H), 8.62 (d, 4H), 8.24 (s, 1H), 7.73 (t, 4H), 7.49–7.41 (m, 6H), 7.31–7.23 (m, 5H), 3.90 (s, 8H), 3.47 (s, 4H). ^{13}C NMR (DMSO-d_6, 300 MHz): δ 170.1, 159.1, 149.8, 139.8, 137.4, 129.8, 123.7, 123.1, 114.7, 110.4, 60.1, 58.6. FABMS *m*/*z* (M^+): calcd 586.69, found, 586.69. Anal. Calcd for $C_{34}H_{34}N_8O_2$ (586.69): C, 69.61; H, 5.84; N, 19.10%. Found: C, 69.37; H, 5.58; N, 19.46%.

4.2.5. 2-Chloroethylamidopyridine. 2-Chloroacetyl chloride (0.39 mL, 5.0 mmol) was dissolved in chloroform (20 mL), then added dropwise to a cooled, stirred solution of 2-aminopyridine (380.2 mg, 4.0 mmol) and pyridine (0.41 mL, 5.0 mmol) in chloroform (20 mL) within 15 min. After stirred for 4 h at room temperature, the liquid was removed under reduced pressure to obtain a pale red-brown solid. It was purified by silica gel column chromatography using DCM/methanol (20:1, v/v) as eluent to afford 537.4 mg (78.7% yield) of product. IR (KBr): 3385 (N–H), 3362 (N–H), 1689 (C=O). ^1H NMR (DMSO-d_6, 300 MHz) δ 10.80 (s, 1H), 8.34 (d, 1H), 8.04 (d, 1H), 7.82 (t, 1H), 7.14 (t, 1H), 4.35 (s, 2H). ^{13}C NMR (DMSO-d_6, 300 MHz): δ 166.5, 151.3, 147.1, 140.5, 120.7, 114.7, 44.0. Anal. Calcd for $C_7H_7ClN_2O$ (170.60): C, 49.28; H, 4.14; N, 16.42%. Found: C, 49.27; H, 4.15; N, 16.42%.

*4.2.6. 2-(Amidomethyl-2,2′-dipicolylamine)pyridine (**ADPA-P**).* 2-Chloroethylamidopyridine(341.2 mg, 2.0 mmol), 2,2′-dipicolylamine (0.57 mL, 3.0 mmol), *N*,*N*-diisopropylethylamine (0.53 mL, 3.0 mmol), and potassium iodide (20 mg) were dissolved in acetonitrile (30 mL). After the solution was stirred and refluxed for 12 h under nitrogen atmosphere, it was cooled to room temperature and placed under reduced pressure. There d-brown oil that was obtained was purified by silica gel column chromatography using DCM/methanol (10:1, v/v) as eluent to afford 579.1 mg (86.8% yield) of product. ^1H NMR (DMSO-d_6, 300 MHz) δ 10.80 (s, 1H), 8.55 (d, 2H), 8.35 (d, 1H), 8.06 (d, 1H), 7.77–7.73 (m, 3H), 7.47 (d, 2H), 7.26 (t, 2H), 7.10 (t, 2H), 3.96 (s, 4H), 3.49 (s, 2H). ^{13}C NMR (DMSO-d_6, 300 MHz): δ 170.9, 159.1, 152.2, 149.6, 148.8, 138.8, 137.3, 123.6, 123.0, 120.1, 113.8, 60.4, 58.5. FABMS *m*/*z* (M^+): calcd 333.39, found, 333.39. Anal. Calcd for $C_{19}H_{19}N_5O$ (333.39): C, 68.45; H, 5.74; N, 21.01%. Found: C, 68.21; H, 5.65; N, 21.34%.

4.3. X-ray crystallography

The diffraction data for **1** were collected on a Bruker SMART AXS diffractometer using Mo Kα (λ=0.71073 Å). The crystal was mounted on a glass fiber under epoxy. The CCD data were integrated and scaled using a Bruker SAINT, and the structures were solved and refined using SHELXTL. Hydrogen atoms were located in the calculated positions. The crystallographic data are listed in Table S1. The selected bond lengths and angles are listed in Table S2. The CIF deposition number: CCDC 806362. CCDC 806362 contains all crystallographic details of this publication and is available free of charge at www.ccdc.cam.ac.uk/conts/retrieving.html or can be ordered from the following address: Cambridge Crystallographic Data Center, 12 Union Road, GB-Cambridge CB21EZ; fax: +44 1223 336 033; or deposit@ccdc.cam.ac.uk.

Crystal data for **BADPA-P**: $C_{33}H_{33}N_9O_2$, M_W=587.68, T=170 K, λ=0.71073 Å, triclinic, $P\bar{1}$, a=9.1396(14) Å, b=12.868(2) Å, c=14.649(2) Å, α=68.976(3)°, β=75.392(3)°, γ=69.902(3)°, V=1493.7(4) $Å^3$, Z=2, D_{calcd}=1.307 Mg/m^3, μ(Mo Kα)=0.086 mm^{-1}, F(000)=620, crystal size, 0.20×0.13×0.10 mm. No. of reflections measured: total, 8369; unique, 5719 (R_{int}=0.0397). Refinement method: full-matrix least-squares on F^2, goodness of fit indicator 0.781, final $R_1[I>2\sigma(I)]$=0.0413.

Acknowledgements

Financial support from Korean Science & Engineering Foundation (2009-0074066), Converging Research Center Program through the National Research Foundation of Korea (NRF) funded by the Ministry of Education, Science and Technology (2009-0082832), and Brigham Young University is gratefully acknowledged.

Supplementary data

Supplementary data including experimental procedures, UV–vis, fluorescence, and NMR spectra, and X-ray crystallography tables. Supplementary data associated with this article can be found, in the online version, at doi:10.1016/j.tet.2011.08.049.

References and notes

1. (a) Lim, N. C.; Freake, H. C.; Brückner, C. *Chem.—Eur. J.* **2005**, *11*, 38; (b) Dai, Z.; Canary, J. W. *New J. Chem.* **2007**, *31*, 1708; (c) Que, E. L.; Eomaille, W.; Chang, C. J. *Chem. Rev.* **2008**, *108*, 1517; (d) Tomat, E.; Lippard, S. J. *Curr. Opin. Chem. Biol.* **2010**, *14*, 225.
2. (a) Zhou, X.; Yu, B.; Guo, Y.; Tang, X.; Zhang, H.; Liu, W. *Inorg. Chem.* **2010**, *49*, 4002; (b) Núñez, C.; Bastida, R.; Macías, A.; Bértolo, E.; Fernandes, L.; Capelo, J. L.; Lodeiro, C. *Tetrahedron* **2009**, *65*, 6179.
3. Zhu, J.-F.; Yuan, H.; Chan, W.-H.; Lee, A. W. M. *Tetrahedron Lett.* **2010**, *51*, 3550.
4. Li, L.; Dang, Y.-Q.; Li, H.-W.; Wang, B.; Wu, Y. *Tetrahedron Lett.* **2010**, *51*, 618.
5. (a) Tamanini, E.; Flavin, K.; Motevalli, M.; Piperno, S.; Gheber, L. A.; Todd, M. H.; Watkinson, M. *Inorg. Chem.* **2010**, *49*, 3789; (b) Ohshima, R.; Kitamura, M.; Morita, A.; Shiro, M.; Yamada, Y.; Ikekita, M.; Kimura, E.; Aoki, S. *Inorg. Chem.* **2010**, *49*, 888.
6. Yu, M.-M.; Li, Z.-X.; Wei, L.-H.; Wei, D.-H.; Tang, M.-S. *Org. Lett.* **2008**, *10*, 5115.
7. Zhou, Y.; Kim, H. N.; Yoon, Y. *Bioorg. Med. Chem. Lett.* **2010**, *20*, 125.
8. Zhang, J. F.; Bhuniya, S.; Lee, Y. H.; Bae, C.; Lee, J. H.; Kim, J. S. *Tetrahedron Lett.* **2010**, *51*, 3719.
9. Lee, D. Y.; Singh, N.; Kim, M. J.; Jang, D. O. *Tetrahedron* **2010**, *66*, 7965.
10. Smith, B. A.; Akers, W. J.; Leevy, W. M.; Lampkins, A. J.; Xiao, S.; Wolter, W.; Suckow, M. A.; Achilefu, S.; Smith, B. D. *J. Am. Chem. Soc.* **2010**, *132*, 67.
11. Xu, Z.; Baek, K.-H.; Kim, H. N.; Cui, J.; Qian, X.; Spring, D. R.; Shin, I.; Yoon, J. *J. Am. Chem. Soc.* **2010**, *132*, 601.
12. Wang, H.-H.; Gan, Q.; Wang, X.-J.; Xue, L.; Liu, S.-H.; Jiang, H. *Org. Lett.* **2007**, *9*, 4995.
13. Xue, L.; Liu, C.; Jiang, H. *Chem. Commun.* **2009**, 1061.
14. Chen, X.-Y.; Shi, J.; Li, Y.-M.; Wang, F. L.; Wu, X.; Guo, Q. X.; Liu, L. *Org. Lett.* **2009**, *11*, 4426.
15. Xue, L.; Liu, Q.; Jiang, H. *Org. Lett.* **2009**, *11*, 3454.
16. Hanaoka, K.; Muramatsu, Y.; Urano, Y.; Terai, T.; Nagano, T. *Chem.—Eur. J.* **2010**, *16*, 568.
17. Liu, Z.; Zhang, C.; Li, Y.; Wu, Z.; Qian, F.; Yang, X.; He, W.; Gao, X.; Guo, Z. *Org. Lett.* **2009**, *11*, 795.
18. Lee, A. E.; Grace, M. R.; Meyer, A. G.; Tuck, K. L. *Tetrahedron Lett.* **2010**, *51*, 1161.
19. (a) Ojida, A.; Mito-oka, Y.; Sada, K.; Hamachi, I. *J. Am. Chem. Soc.* **2004**, *126*, 2454; (b) Ojida, A.; Inoue, M.; Mito-oka, Y.; Tsutsumi, H.; Sada, K.; Hamachi, I. *J. Am. Chem. Soc.* **2006**, *128*, 2052; (c) Ojida, A.; Sakamoto, T.; Inoue, M.; Fujishima, S.; Lippens, G.; Hamachi, I. *J. Am. Chem. Soc.* **2009**, *131*, 6543; (d) Mangalum, A.; Smith, R. *Tetrahedron* **2009**, *65*, 4298; (e) Mohamed, M.; Neverov, A. A.; Brown, R. S. *Inorg. Chem.* **2009**, *48*, 11425.
20. Nolan, E. M.; Lippard, S. J. *Acc. Chem. Res.* **2009**, *42*, 193.
21. CCDC-806362 contains all crystallographic details and is available free of charge at www.ccdc.cam.ac.uk/conts/retrieving.html.
22. Marlin, D. S.; Cabrera, D. G.; Leigh, D. A.; Slawin, A. M. Z. *Angew. Chem., Int. Ed.* **2006**, *45*, 77.